Supplementary Information Section

Dry Electrodes with a Printed Cellulose-Graphene Ink for Low-Profile Strain Sensors in Electromyography

Allyson R. Tesky[1], McKenna Hicks[2], Sujan Aryal[3], Brendan Jones[3], Julia Molitor[4], and Anupama B. Kaul[3,5]*

[1]Department of Biomedical Engineering, [2]Department of Computer Science and Engineering [3]Department of Electrical Engineering, [4]Department of Mechanical Engineering, [5]Department of Materials Science and Engineering, University of North Texas, Denton, TX 76203, U.S.A.

*Corresponding Author Email: anupama.kaul@unt.edu

1. Commercial electrode evaluation and EMG collection

We started our study to explore the transduction and collection of EMG signals using commercially available electrodes, where a single channel electromyograph breadboard circuit was developed in order to collect EMG signals. The circuit diagram for this detection scheme is pictured in **Figure S1(a)**, where the INA 126 operational amplifier and TL 7660 voltage rectifier are shown in a bipolar electrode configuration with matching resistive networks to optimize the gain. The proximity of the bipolar electrodes and preparation of the skin prior to placement provide similar skin-electrode impedance[S1], and therefore much of the associated noise from this interface is removed with the common-mode rejection of the associated instrumentation amplifiers. Traditionally, electromyographs utilize on-board band-pass filtering[S1,S2] and/or digital filtering techniques[S3,S4]. While filtering is preferable for signal analysis, the largest contaminant tends to be power line noise at 60 Hz, which may occasionally be removed via a notch filter, but due to the majority of the EMG signal lying in the 10-250 Hz band[S4], filtering to remove the power line noise is not recommended[S1,S3,S4]. For these reasons, the common-mode noise removal between the

bipolar electrodes is considered sufficient for prototype purposes, as visible signals can be acquired with adequate gain resistors interfaced to the instrumentation amplifiers.

The single-channel circuit in **Figure S1(a)** allows for measurements on any muscle group large enough to accommodate the pair of commercial Ag/AgCl 3M™ gel electrodes. Because the biceps brachii are easy to locate, access, and activate, they were selected as the muscle of choice for our baseline experiments with EMG. The motion path of the arm during activation of the biceps can be seen in **Figure S1(b)**, from the relaxed to the curled state, where movement primarily takes place in the sagittal plane with minimal lateral movement in the coronal plane. While there are different methods and reasoning for some electrode placements over others, it is generally recommended that electrodes be located on the motor units longitudinally on the mid-line and away from the tendon, and transversely centered so that the sensors are away from the recording area boundary[S1,S5]. With the electrodes placed, curling of several different dumbbell weights at 2.27, 6.80, and 11.34 kgs (i.e., 5, 15, and 25 lbs.) could be measured to evaluate muscle fiber recruitment. The rectified, unfiltered results, pictured in **Figure S1(c)**, showed higher amplitudes, and thus higher rates of muscle fiber activation with heavier weights, in alignment with expected results from prior EMG studies. Parenthetically, this placement on the biceps brachii may be seen by the schematic representation in the inset of **Figure S1(c)**, where the electrodes for the differential signal, V_{in+} and V_{in-}, are visualized, while the optional ground electrode for the signal V_{gnd} is placed on the bony part of the elbow.

Some studies report adjustment time needed after electrode placement for a good signal-to-noise ratio (SNR) due to electrochemical noise[S3], as well as drawbacks when the electrode dries out[S4,S6]; very few reports go in-depth into the cutoffs and time-dependent usage of the electrodes. Since one of the biggest advantages for dry electrodes over gel electrodes is their long-term

durability independent of usage time without an adjustment period, it was thus important to evaluate the baseline for the commercial gel electrodes in this study, for comparative analysis with emergent technologies. After skin preparation and electrode placement, four basic movements were performed over a 24 hour time frame represented by the data in **Figure S1(d)**, where the right insets illustrate the specific nature of these movements, namely with the arm at rest **(i)**, gentle contraction **(ii)**, 6.80 kg (15 lbs) bicep curl **(iii)**, and forceful contraction **(iv)**. Since there are multiple individually stimulated muscle fibers in each motor unit[S5], collected EMG signals are really several innervated fibers activated at once, and this leads to a characteristic noisy profile dipping from positive to negative. While there are methods to deconvolute and separate these signals[S2,S3], a holistic view of the motor unit can nevertheless be accomplished via a linear envelope through rectification and a moving-average filter[S4], which is sufficient to determine the overall level, given the varying nature of the movements.

To facilitate further comparison, a total of 10 measurements per movement type were taken for each recording period. A 10 second window was permitted for each individual measurement, for which movements were initiated at the 2 second mark where applicable (i.e., for all movements save for "rest"), held at the apex of the movement for 2 seconds, and then released and relaxed for 2.5 seconds. To eliminate variation between initiation time, the sets of 10 movements were aligned by rising edge in MATLAB, rectified, and their linear envelopes averaged. These averaged linear envelopes are used for all subsequent analysis.

Shown in **Figure S1(d)**, many of the signals appeared to be of a similar amplitude except for the signals during rest and gentle contractions at 4 hours, and during the forceful contraction immediately after placement. It is notable that these amplitudes are higher, particularly when the arm is at rest, as the output voltage during rest is a result of both the line/circuit noise, as well as

the noise generated at the skin-electrode interface. During movements of higher recruitment, the resulting EMG signal had a similarly higher amplitude above the noise levels, and moving averages were similar across all other time frames. Results with the moving average taken over the time interval up to 24 hours were summarized through the signal-to-noise (SNR) ratio calculation, shown in **Figure S1(e).** This analysis indicated that the lowest SNR occurs after 4 hours of placement, suggesting the gel had begun to dry out, but still needed time for adjustment to the skin to produce sweat at the interface for good conductivity[S6]. The SNR improved at the 1-hour mark after forming an initial seal and the highest SNR was observed at 8 hours. While the signal during the forceful contraction was weakest immediately upon placement, the corresponding noise floor was comparable to other timeframes—this contrasts with the noise floor at 4 hours, which was higher than any other period, indicating weakening at the skin-electrode interface.

These results support previous findings[S1,S7] which allude to the high acclimatization time needed for commercial gel electrodes to yield a good connection at the skin-electrode interface, facilitated through sweat production intermixing with the electrolytic gel. Although commercial gel electrodes remain the gold standard for electrophysiological measurements of the body, they nonetheless possess numerous downsides that make their use less practical. Even with proper preparation of the skin prior to placement, the response of the electrodes will change over time, and may therefore be unreliable for situations where extended duration studies are needed. Dry electrodes can thus circumvent these issues, although with a typically higher impedance at the skin-electrode interface[S1]. Despite this, they generally tend to be more consistent over longer durations, as we also demonstrate through our strain-based sensing devices developed with our Cyrene-based graphene inks.

2. Electromyography collection and analysis

The electrodes were placed onto a cleaned surface, side-by-side, so that the gel conducting portions would be as close as possible (about 3 cm, center-to-center) for both consistency between measurements and clarity of the gathered signal. An optional third electrode was placed over the bony part of the elbow where muscle activation should not be observed and connected to the common ground. After electrodes were placed, they were pressed on to promote adhesion, and the leads connecting the electrodes to the breadboard circuit shown in **Figure S1(a)**, were attached. While the red lead was always used for V_{in+} and connected to the medial electrode (as in **Figure S1(c)),** these electrode leads could be switched without divergence in results due to the rapid polarity switching innate to the EMG and rectification of results. Electrical signals were viewed and saved via a Tektronix TDS 2024C oscilloscope and then subsequently analyzed in MATLAB.

Most measurements were taken soon after electrode placement and removed upon completion of the experiment. An exception to this was the 24 hour SNR analysis, **Figure S1(e)** and **(f)**, which involved active electrodes for the full duration of the experiment before removal. All movements for the EMG tests followed the same basic path seen in **Figure S1(b)**. The four movement types were repeated in sequence of rest, gentle contraction, 6.80 kg (15 lb) bicep curl, and forceful contraction for a total of 10 measurements each at lengthening intervals over the course of 24 hours to evaluate the SNR changes of the electrode over time. For the analysis of these results in MATLAB, the noise profile of each time period was taken at rest, where no muscular activation was occurring. These were used to denoise the other signals for a clean EMG result, which could then be used for an approximation of the SNR[S2-S4].

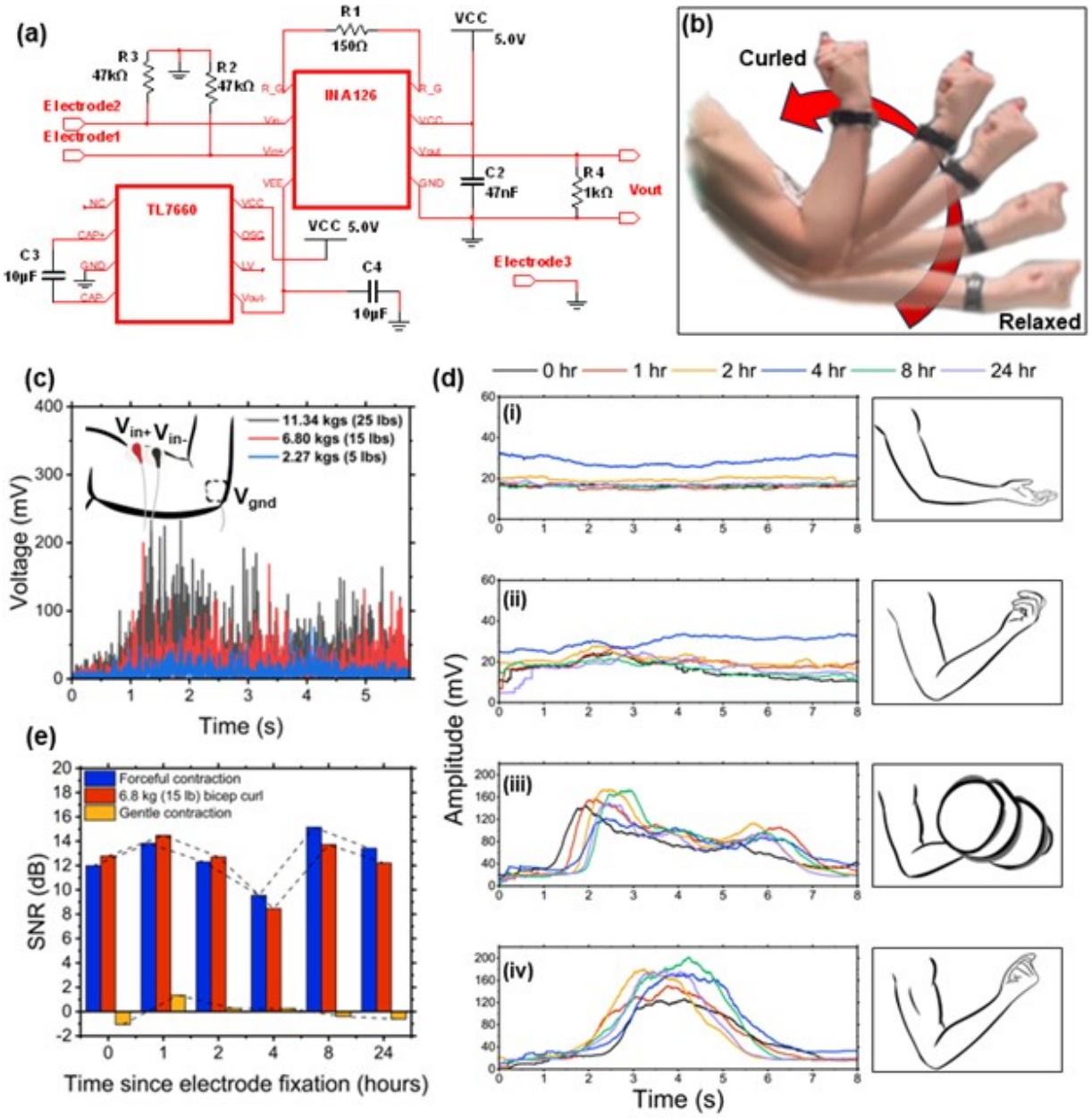

Figure S1: (a) Circuit diagram of the EMG recording device designed for a dual-channel configuration. **(b)** Motion path of arm during contractile movements. **(c)** Rectified EMG measurements taken during bicep curls show higher amplitudes under higher loads. Inset shows bipolar electrode placement on biceps brachii and the ground electrode on the bony part of the elbow. **(d)** Moving averages of basic movements at time intervals from 0 to 24 hours after electrode positioning. **(e)** SNR of basic movements at time intervals from 0 to 24 hours after electrode positioning, showing the highest SNR up to 8 hours after placement.

3. Temperature-dependent Raman analysis on printed graphene films and transport measurements

Further characterization was performed on the Cyrene-based graphene through temperature-dependent Raman spectroscopy conducted from 77 to 800 K in atmospheric air to decipher how the phonon spectra are modulated and possible interactions of phonons with defects, while at the same time shedding insights into their mechanical and thermal robustness in extreme environments. Naturally, some changes are expected to occur throughout a single cooling to heating cycle in most materials, and to evaluate these changes, it can be helpful to reverse the cycle from 800 to 77 K. In doing this, the material can be examined for hysteresis and temperature-related degradation. The difference in the Raman shift, as seen in **Figure S2**, and the full-width-at-half-maximum (FWHM), as shown in **Figure S3**, of the peaks between the cooling or heating cycle appeared insignificant, indicating little hysteresis in the data.

Four locations on the sample were selected and measurements were taken in each location by moving the laser spot to separate locations, before altering the temperature for the next set of temperature-dependent measurements. The sample was allowed to reach steady-state and equilibrate at its new temperature, prior to acquiring the data and this methodology was used from 77 K to 800 K in the rising cycle, and again from 800 K to 77 K in the temperature descending cycle. The data were averaged for the peak locations over the four sites during both cycles, from which the standard deviation σ was calculated which is reflected in the error bars, seen in **Figures S2** and **S3**.

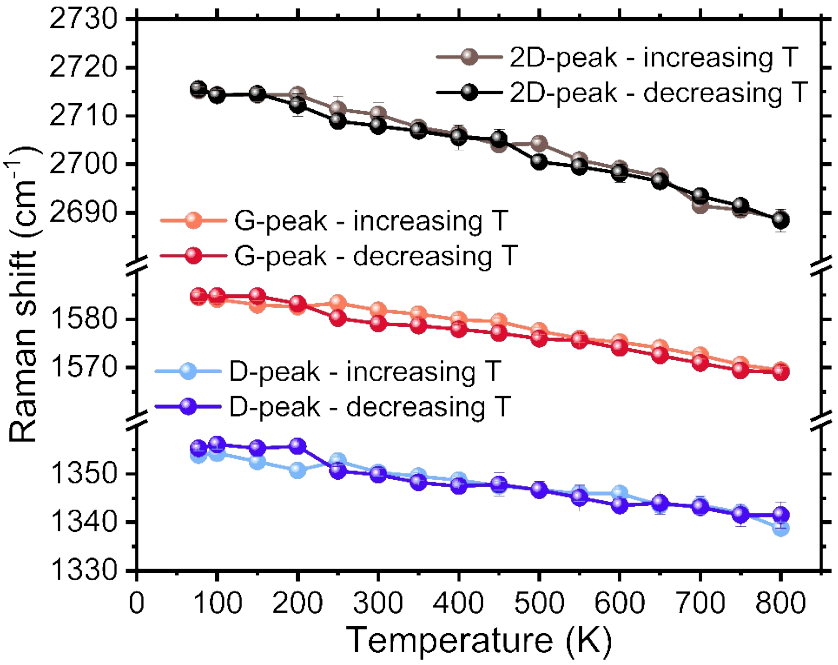

Figure S2: Raman shift of the *D-, G-,* and *2D*-peaks demonstrated a similar behavior in the forward (forward) and reverse (cooling) thermal cycles, suggesting minimal hysteresis present. In both

cases, the 2D-peak experienced the largest shift of ~ 25-35 cm^{-1}, corresponding to a red-shift as temperature increased. Error bars represent *1-σ* variations about the mean.

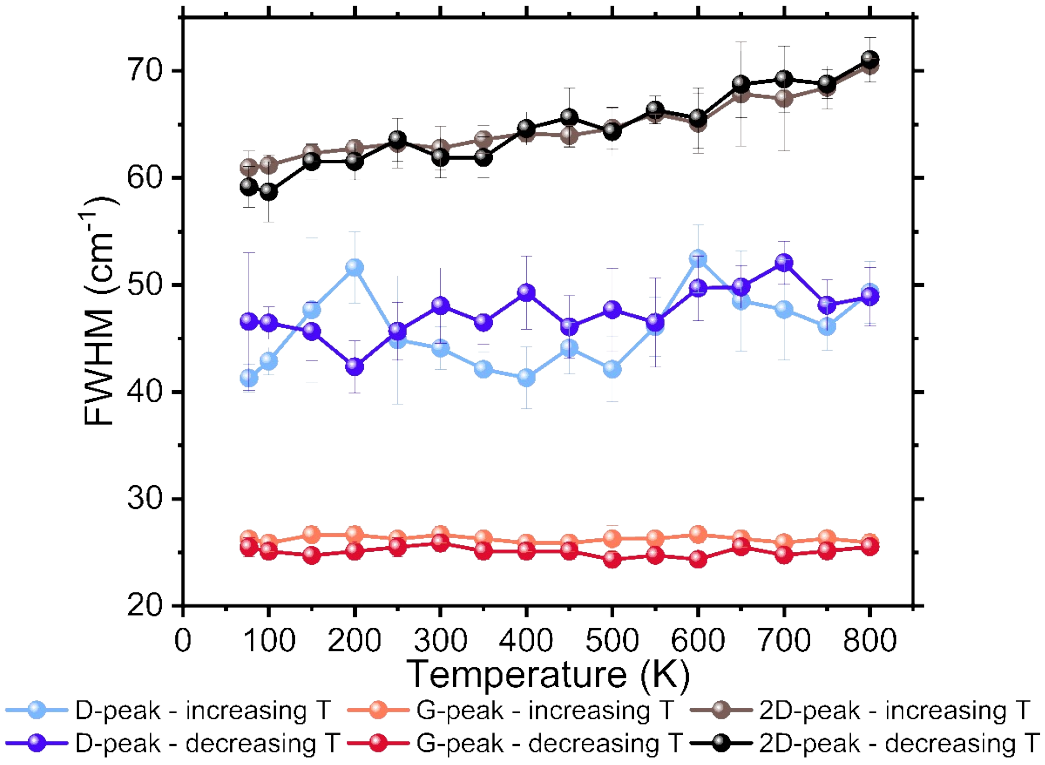

Figure S3: The FWHM of the *D-, G-,* and *2D*-peaks of the graphene film at increasing temperature in light red, blue, and purple plots, respectively, while the corresponding cooling cycle data are shown in dark red, blue, and purple, respectively. The data reveals a largely temperature invariant FWHM, with the exception of the 2D-peak, and minimal hysteresis between the heating and cooling cycles. Error bars represent *1-σ* variations about the mean.

The data in **Figure S4** provides the *I-V* sweeps from -20 V to +20 V over the 4 K to 350 K range, where the current compliance was set at ~ 1 mA, for the graphene films on **(a)** SiO_2/Si and **(b)** PI substrates. The *I-V* response shows the wider spread of the currents on the SiO_2/Si substrates compared to the film on the PI substrate, which likely arises from differences in film morphology between the two substrates.

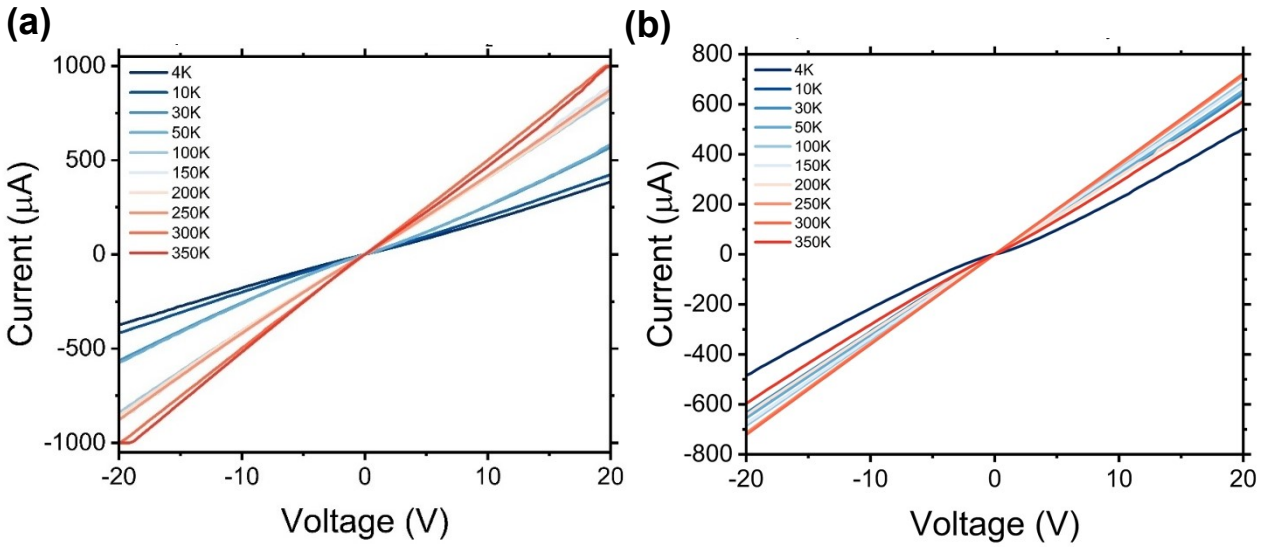

Figure S4: Temperature-dependent DC transport measurements over multiple temperatures, corresponding to the data in **Figure 3(a)** of the main manuscript for graphene inkjet-printed on **(a)** SiO_2/Si substrate, and **(b)** PI substrate.

One of the characteristic Raman peaks ascribed to the presence of the CAB additive[S8] occurs at a Raman wavenumber of ~ 2937 cm^{-1}, similar to spectra gathered for the graphene ink as in prior work[S9]. The spectra of the Cyrene-based ink that used the CAB in **Figure S5(a)**, shows the characteristics peaks at room temperature over the **(i)** full spectral range from 1000 – 3000 cm^{-1}, while in **(ii)** an enlarged region from 2880 – 3000 cm^{-1} is shown which reveals the presence of the CAB characteristic peak at ~ 2940 cm^{-1}. While this peak can still be observed as temperature is varied, the intensity of the peak is far lower when compared to the dominant graphitic D-, G- and 2D-peaks. Additionally, there appears to be little discernable variation in the peak location as a function of temperature, illustrated by the data in **Figure S5(b)**, unlike the red-shifts clearly evident for the graphitic peaks. Moreover, the intensity of this peak as a function of temperature, captured by the data in **Figure S5(c)**, also shows a largely temperature invariant response; its far lower intensity likely suggests the CAB has denatured and decomposed, likely arising from the temperatures used in the graphene film annealing process, as intended.

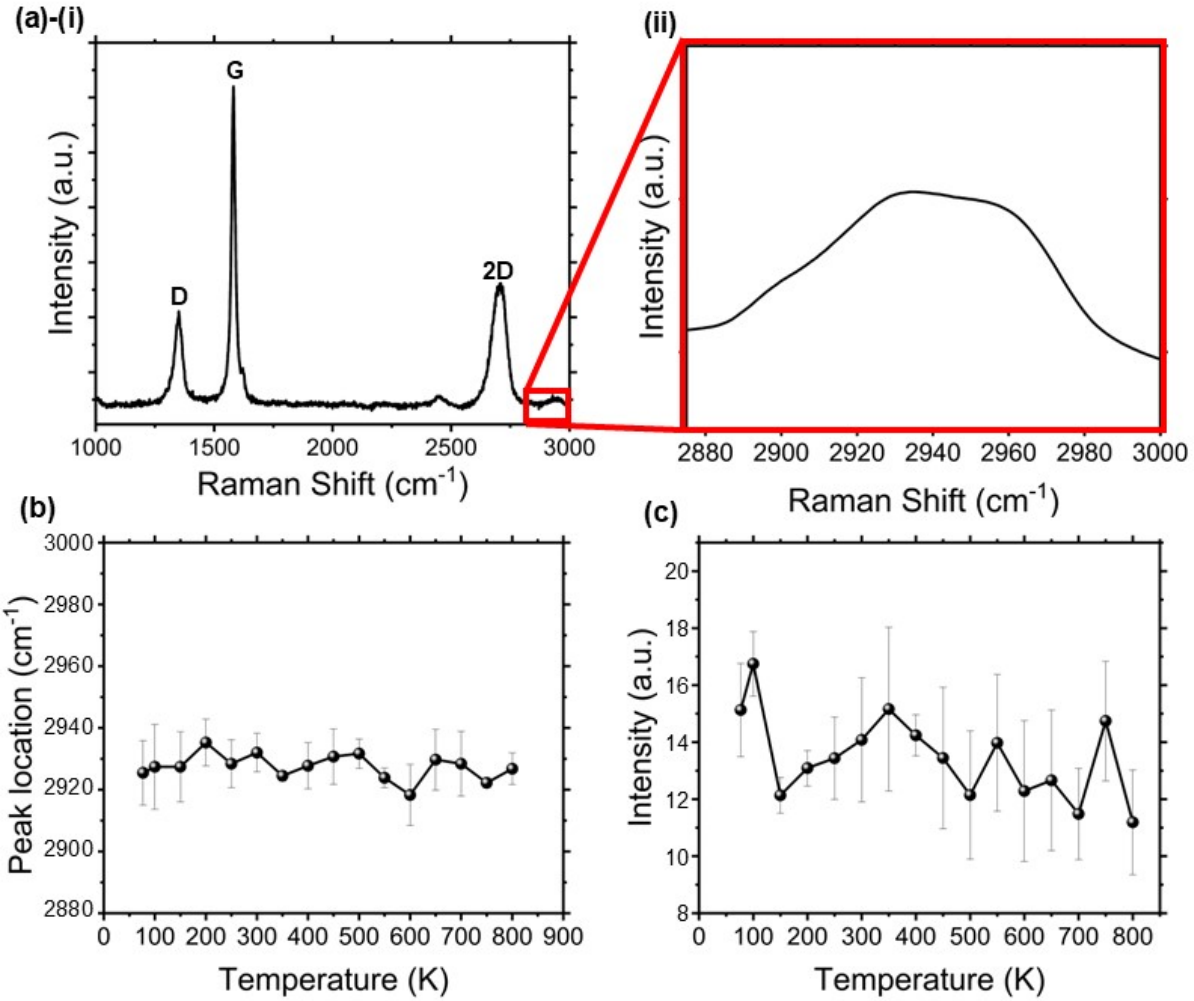

Figure S5: (a) Room-temperature Raman spectra of the C/T and Cyrene inks corresponding to **Figure 1(a)** of the main manuscript with (i) the full spectrum and (ii) the typical location of the

CAB peak. Temperature-dependent Raman spectra of the pure-CAB dispersed on SiO_2/Si with **(b)** and **(c)** demonstrating a largely temperature invariant behavior of the Raman peak position and peak intensity, respectively. This suggests the CAB may already have decomposed from the routine annealing conducted during the graphene film device processing and fabrication. Error bars represent 1-σ variations about the mean.

References

S1. R. Merletti, M. Aventaggiato, A. Botter, A. Holobar, H. Marateb, and T. M. Vieira, *Crit. Rev. Biomed.* Eng. 2010, **38**, 305-45.

S2. M. B. I. Raez, M. S. Hussain and F. Mohd-Yasin, *Biological Procedures Online,* 2006, **8,** 11–35.

S3. M. Boyer, L. Bouyer, J. Roy and A. Campeau-Lecours, *Sensors,* 2023, **23,** 2927.

S4. D. Esposito, J. Centracchio, P. Bifulco and E. Andreozzi, *Sci Rep,* 2023, **13,** 7768.

S5. I. Y. Kuo and B. E. Ehrlich, *Cold Spring Harbor Perspectives in Biology,* 2015, **7,** a006023.

S6. B. Ali, H. Cheraghi Bidsorkhi, A. G. D'Aloia, M. Laracca and M. S. Sarto, *Sensors and Actuators Reports,* 2023, **5,** 100161.

S7. F. J. Romero, E. Castillo, A. Rivadeneyra, A. Toral-Lopez, M. Becherer, F. G. Ruiz, N. Rodriguez and D. P. Morales, *Npj Flex Electron,* 2019, **3,** 1–6.

S8. D. Marlina, M. Novita, M. T. Anwar, H. Kusumo and H. Sato, Journal of Physics. Conference Series, 2021, 1869, 12006.

S9. K. Pan, Y. Fan, T. Leng, J. Li, Z. Xin, J. Zhang, L. Hao, J. Gallop, K. S. Novoselov and Z. Hu, Nat Commun, 2018, 9, 5197–10.